RADIOMETRIC CALIBRATION OF SAR IMAGE DATA

A. Freeman

Jet Propulsion Laboratory
California Institute of Technology
M/S 300-235, 4800 Oak Grove Drive
Pasadena, CA 91109

Tel: (818) 354-1887
Fax: (818) 393-6943

ABSTRACT:

Recent advances in calibration techniques have made calibrated SAR images, in which the data represents radar cross-section (σ) or normalized radar cross-section (σ^o), a reality. In this paper, some of these recent advances are discussed, in the context of their impact on SAR system design, and in terms of the errors associated with each technique.

The main sources of error in radiometric calibration of SAR data are fluctuations in the transmitted power, receiver gains, system noise and the illumination pattern of the antenna. Internal calibration loops can be used to ensure the stability of the transmitters and receivers. The noise level can be measured by turning off the transmitters and operating in a receive-only mode. One of the more difficult problems remaining is then to determine the appropriate antenna pattern illumination for each pixel on the ground. This can be achieved by a variety of techniques: first, the normal antenna pattern can be measured using a suitable uniform, distributed target such as the Amazon Rain Forest; second, the roll angle of the antenna can be measured by using some form of echo-tracker; then the elevation angle for each pixel can be determined if the terrain height variations in the image are known or can be bounded. For a spaceborne SAR, a curved earth model gives a good approximation for the long range at which spaceborne SAR's must operate. For an airborne SAR, a Digital Elevation Model (DEM), registered to the SAR image, may be necessary. The DEM can be derived from a standard topographic data set, registered using tie-points to the SAR image, or from interferometric SAR height maps which are automatically registered to the SAR image, or by monopulse techniques, which are also in the same reference frame as the SAR image. Additionally, these three techniques may be used to determine the local incidence angle for each pixel, so that measurements of σ may be converted to σ^o.

To verify radiometric calibration, and particularly to ensure that the data is absolutely calibrated, known calibration targets such as corner reflectors or transponders, are often used. These suffer from their own calibration uncertainties, which may be a limiting factor in the overall radiometric calibration.

Examples will be presented from the NASA/JPL AIRSAR and ERS-1.

KEY WORDS: Synthetic Aperture Radar (SAR), Calibration, Radar Cross Section measurement

1. INTRODUCTION

Synthetic Aperture Radar (SAR) was first developed in the 1950's (Wiley, 1954) , for long-range mapping and surveillance from airborne platforms. During the 1960's, the first civilian application of SAR, for geological mapping, was demonstrated. In 1978, the launch of SEASAT (Ford, 1980) proved that a spaceborne SAR could be very effective in monitoring the Earth's surface. By the present date, the field has matured to the point where several space agencies throughout the world have already launched or are poised to launch their own spaceborne SAR sensor into orbit (Attema, 1991; Elachi, 1991; Johnson, 1991; Jordan, 1991; Nemoto et al, 1991; Raney et al, 1991), and airborne SAR's for remote sensing abound. A new generation of non-military SAR sensors is coming into existence, designed to be operationally stable, equipped with capabilities such as multi-frequency, multipolarization data-collection, interferometric modes and wide-swath coverage. The list of applications for SAR as a remote sensing tool is also rapidly expanding in fields as diverse as oceanography, forestry, sea-ice monitoring, planetary exploration, geology, agriculture and terrain mapping.

In earlier years, calibration of SAR image data was not a priority. With the new generation of SAR sensors, calibrated SAR imagery is rapidly becoming the norm, and can be directly related to the radar backscatter of the scene, e.g., via a look-up table relating image pixel number to radar backscatter value, which can then be provided to the applications scientist. Calibrated SAR image products should be repeatable from day to day, and from frame to frame; stable, within an image frame and between channels, and its accuracy known and understood.

Much has been achieved in the microwave remote sensing field with uncalibrated SAR images. The success of the SEASAT SAR (Ford, 1980) is a case in point. However, the quantitative use of SAR data, as opposed to the qualitative, requires calibrated images. We have reached a stage where the applications scientist who wants to compare data from different sensors, extract geophysical parameters from backscatter measurements using models, carry out multi-temporal studies over large areas, build up a database of backscatter measurements for different types of terrain/incidence angle, etc., can only do so using calibrated SAR data products. Also, the full benefit of the new multichannel SAR's will not be felt unless the different channels can be properly compared with one another (Freeman et al, 1988). Certain types of backscatter phenomena can be readily understood if calibrated polarimetric SAR data is available. Another concern is that the SAR data-gathering and processing operations should be transparent to the user, so that the applications scientist does not have to spend his time checking whether the data he has received are of adequate quality for his purposes.

2. SAR DATA CALIBRATION

High-resolution radar measurements

A SAR system is a high-resolution radar, capable of measuring the (real or complex) radar reflectivity of a surface. SAR's usually operate as monostatic radars, mounted on a moving platform, with an antenna looking out and down towards one (or both) sides relative to the platform motion vector. In its ideal realization, a SAR image should just represent the scattering matrix element, S_{pq}, in complex representation,

or the radar cross-section, σ_{pq}, in intensity, for the receive (q) and transmit (p) polarizations of the radar. The scattering matrix is defined via (Ulaby and Elachi, 1990):

$$\begin{pmatrix} E_h^s \\ E_v^s \end{pmatrix} = \frac{e^{jk_oR}}{R} \begin{pmatrix} S_{hh} & S_{vh} \\ S_{hv} & S_{vv} \end{pmatrix} \begin{pmatrix} E_h^i \\ E_v^i \end{pmatrix} \quad (1)$$

where $\begin{pmatrix} E_h^i \\ E_v^i \end{pmatrix}$ is the electric field vector of the wave incident on the scatterer, $\begin{pmatrix} E_h^s \\ E_v^s \end{pmatrix}$ is the electric field vector of the scattered wave, k_o is the wavenumber of the iluminating wave, and R the (radial) distance between the scatterer and the radar antenna. The radar cross-section (RCS) is related to the scattering matrix via:

$$\sigma_{pq} = 4\pi |S_{pq}|^2 \quad (2)$$

Here only linear polarizations (horizontal, h or vertical, v) are considered, since most SAR systems just measure linear polarizations. It is possible to define and measure RCS for all possible polarizations, however, such as right- and left-hand circular (Ulaby and Elachi, 1991).

Expressions (1) and (2) above represent the quantities which are directly measurable by a SAR. The units for σ_{pq} are in meters squared. Both σ_{pq} and S_{pq} are functions of spatial position (x, y), time (t), viewing geometry (θ, ϕ), and radar wavelength (λ) in addition to the polarizations of the transmitted and received electromagnetic waves. Each image pixel value should correspond to an accurate and precise measurement of one of these quantities, and be repeatable, under the same conditions, by that or another radar sensor.

Two other measurements of the radar backscatter properties are often derived from σ_{pq}. They are the normalized radar cross-section,

$$\sigma^o_{pq} = \frac{\sigma_{pq}}{A} \quad (3)$$

where A is the area of the pixel projected onto the ground, and

$$\gamma^o_{pq} = \frac{\sigma^o_{pq}}{\cos\theta_i} \quad (4)$$

where θ_i is the local incidence angle at the scattering surface. Note that,

$$A = \frac{p_a p_r}{\sin\theta_i} \quad (5)$$

where p_a and p_r are the SAR image pixel dimensions in azimuth (sometimes referred to as across-track) and slant range (sometimes

referred to as along-track), which are the 'natural' measurement coordinate system of most SAR sensors. The important point to note is that to estimate both γ^o_{pq} and σ^o_{pq} from σ_{pq}, knowledge of the local incidence angle of the scattering surface is required. Often, a flat or curved Earth is assumed when estimating γ^o_{pq} and σ^o_{pq}, but this may not be adequate when imaging a surface with significant terrain height variations.

SAR image formulation

All images, whatever their source, are imperfect, being a blurred representation of reality, with noise superimposed. SAR images are no different, and a convenient mathematical description of a complex (i.e. containing both amplitude and phase information) SAR image is as follows:

$$V(x,y) = \sqrt{K_s}\, e^{j\phi_s}\, S_{pq}(x,y) \otimes h(x,y) + \sqrt{K_n}\, n(x,y) \qquad (6)$$

where V is the measured voltage, x and y are spatial position coordinates within the image, h is a (spatially variant) two-dimensional image blurring function, often referred to as an impulse response function and $\otimes$ denotes convolution in both x and y. The form of the impulse response function depends on the characteristics of the radar sensor, e.g. the form of the transmitted radar pulse, and on the transfer function of the SAR correlator which turns the 'raw' data collected into an image. K_S and ϕ_S represent the gain and phase imposed by the radar on the backscatter measurement, S_{pq}. Both may be functions of x and y. K_S and ϕ_S contain contributions from many sources, including the radar transmitter(s), receiver(s) and the SAR correlator. The term n(x, y) in (6) represents the additive noise present in the backscatter measurements. It is usually assumed to be white and Gaussian in nature and has zero mean. The radar gain term for the noise, K_n, is different than that for the signal because the noise and signal bandwidths may be different (Raney, 1980). The noise phase is usually assumed to be random, uniformly distributed between $-\pi$ and $+\pi$.

It is also possible to formulate an expression for a square-law detected image, which is just the magnitude squared of the complex representation in equation (6). Many SAR images are also multi-looked, in which an incoherent averaging process (e.g. a box filter) is applied to the square-law detected image in order to reduce the speckle variance. In both these representations the phase information is lost and the measurable quantity is σ_{pq} instead of S_{pq}. Both forms still contain noise and system gain terms, however.

To completely calibrate a complex SAR image, it is necessary to determine and correct for the terms $K_S(x, y)$ and $\phi_S(x, y)$, as well as the noise contribution term, $\sqrt{K_n}\, n(x,y)$. (Gray et al, 1990) have shown that, under certain constraints, the form of the impulse response function, h(x, y) does not enter into the calibration problem. For many applications, phase calibration of the SAR data is not required, so that the $\phi_S(x, y)$ term need not be estimated or corrected for. To determine the appropriate correction factors to calibrate a SAR image two basic approaches are used: internal calibration and external calibration. In internal calibration the radar system is characterized a piece at a time by a series of internal calibration measurements, in which stable reference signals are input to some part of the system, and the output response at some other part of the system measured. In external calibration, calibration devices such as corner reflectors or radar transponders, with known RCS behavior, are deployed within the area imaged by the SAR. The responses of these calibration targets within the SAR image are then used to directly determine $K_S(x, y)$ and $\phi_S(x, y)$ and $\sqrt{K_n}\, n(x,y)$.

Internal Calibration

So far, we have discussed the quantities measured by a SAR sensor, and the properties of SAR images. We have not addressed the calibration impact of the process of collecting 'raw' SAR data, nor the SAR image formation process, which turns the 'raw' data into a SAR image. For radiometric calibration, the effects of these processes are combined into two gain terms, K_S and K_n, which were incorporated into the mathematical representation of the complex SAR image, given in equation (6). A convenient form for the overall radar gain term, K_S, as applied to the backscatter signal, is:

$$K_s = \frac{P_t\, G_t^A(\theta_{el},\theta_{az})\, G_r^A(\theta_{el},\theta_{az})\, \lambda^2\, G_r^E\, G_p(x,y)}{(4\pi)^3\, R^4\, L_s\, L_a} \qquad (7)$$

For a calibrated SAR image, K_S should equal one. This places a heavy burden on the SAR processor, since the overall processor gain $G_p(x,y)$ must be adjusted to compensate for all the other terms (Freeman and Curlander, 1989). Measurement of the individual terms in (7), which represent various contributions to the overall radar gain from different sub-systems, by a combination of pre-flight and in-flight tests,

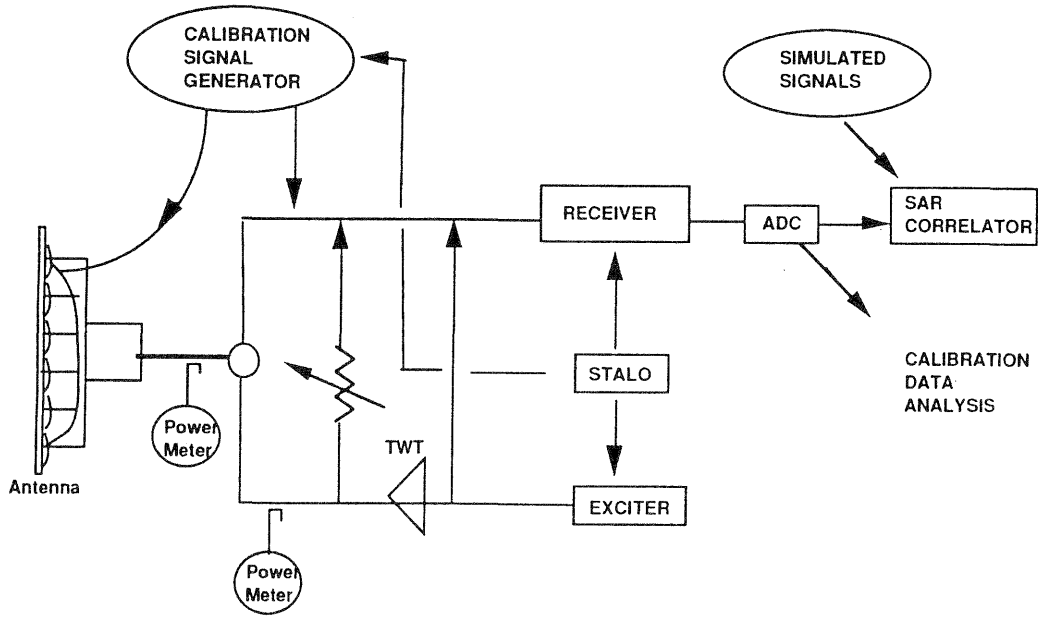

Figure 1. Generic block diagram of a SAR system, showing calibration loops

and subsequent compensation in the SAR processor, is often termed internal calibration (Currie, 1984). In Figure 1 we show a generic form of SAR system configuration, which includes several 'calibration loops' for internal calibration.

Many different approaches are possible for internal calibration of SAR systems. Examining each of the individual terms in (19), the peak transmitted power, P_t, of the radar sensor can often be measured using a power meter, in which case the accuracy and precision of that instrument becomes a factor in the overall calibration accuracy and precision. The two antenna gain terms, $G_t^A(\theta_{el},\theta_{az})$ and $G_r^A(\theta_{el},\theta_{az})$, corresponding to the transmit and receive antennas, are functions of the elevation and azimuth angle θ_{el},θ_{az} at which a given target is observed, and are major sources of calibration uncertainty. The antenna patterns must be known very precisely. This can be achieved to a degree by pre-flight measurements but the patterns may change once mounted on the platform and subjected to the harsh environment of space or a high-flying aircraft . The patterns must, therefore, be re-measured in flight. Knowledge of the patterns themselves is not sufficient: the angles, θ_{el},θ_{az} , at which each point on the ground is illuminated must also be known. This requires knowledge of the pointing in elevation and azimuth of the real beam, which may change due to platform motion. Some form of roll-angle tracker (Freeman et al, 1988) may be necessary to do this. Then, to correct for the antenna pattern variation across a SAR image, we have to convert from the elevation/azimuth coordinates in which the antenna gain patterns are measured to the slant range/azimuth coordinate system of the SAR image. This may not be straightforward, particularly for airborne SAR's, and the traditional flat or curved Earth approximations may lead to large calibration errors. The radar wavelength, λ, can be determined by preflight system tests. The electronic gain in the radar receiver, G_r^E, can also be tested before launch but should be verified in flight using a known signal, such as a sine wave or noise source or a chirp, injected into the receiver front-end at RF or IF frequencies. A system loss term, L_s, is included in (7) to account for attenuation due to cables, etc. Propagation through the atmosphere may also cause attenuation, L_a. Models of radar propagation usually predict small attenuation except at shorter wavelengths (e.g. X-Band) in the presence of rain. The range delay between radar and target, R, can be calibrated if the electronic delays through the radar system are known, and the system timing is calibrated pre-flight.

The processor gain, G_p, can be a major source of error. To begin with, the terms in the processor gain which are invariant must be calibrated by injecting simulated data to determine the relationship between mean power in versus mean power out for the processor. Any range dependence in the processor gain should also be calibrated in this way (Freeman and Curlander, 1989). The processor may perform many functions, besides the basic SAR correlation. An

error in any of the algorithms involved, e.g. radiometric correction for some of the other terms in (7), Doppler tracking, elevation angle tracking, range cell migration correction, PRF ambiguity resolution, look extraction, slant-to ground range conversion, could lead to an error in the radiometric calibration of the final image product.

Our formulation of the mathematical representation of a complex SAR image in equation (6) included a noise term, n(x, y) and a system gain in the presence of noise, K_n. The logical point at which to measure the noise is at the 'raw' data stage, i.e. before SAR processing. At this stage the noise includes contributions from all the dominant noise sources including the Earth's microwave background radiation, thermal noise in the antenna, thermal noise in the receivers and quantization noise due to the analog-to-digital conversion process. This noise can be measured by operating the radar in a receive-only mode, either by turning off the transmitters or recording data before the first ground echo is expected. By passing such noise-only signals through the SAR processor, the system gain in the presence of noise, K_n, which is really just the processor gain in the presence of noise, can be evaluated.

The noise present in a complex SAR image (Equation (6)) provides an additional uncertainty in estimating S_{pq} . This error due to noise has zero mean value but non-zero standard deviation. For square-law detected images (including multi-looked images), the noise affects the estimation of σ_{pq} for each pixel as both a (non-zero) bias and an rms uncertainty on each measurement. The bias could be removed by first measuring the level of image noise as described above, then subtracting it off each σ_{pq} measurement. The remaining rms uncertainty can be reduced (but not completely eliminated) by non-coherent averaging (i.e. multi-looking), just as the variation due to speckle in radar measurements can be reduced.

Internal calibration, as described above, can provide sufficient information to calibrate SAR image data on its own. It is very difficult, however, to completely tie down all the losses and gains in any SAR system and often external calibration, using targets with known scattering characteristics, is used to complete the calibration process (Currie, 1984). In any event, external calibration should be used as a way to verify whether the SAR data from a particular sensor is calibrated.

An alternative approach for estimating K_S is to use the signatures of distributed targets of known RCS (Moore and Hemmat, 1988). The assumption is that the area in question is uniform, and that it's average RCS for the particular radar frequency, polarization, viewing geometry and time of year is known. The procedure involves spatial averaging of the image pixel power measurements to reduce the natural speckle variance in the scene (which can cause errors in measuring K_S), then an estimate of the average noise level must be subtracted off. From there, if the average RCS is known, it is relatively straightforward to estimate K_S or at least the changes in K_S across an image. This approach has been quite successful in determining the relative calibration errors within an image, and has been proposed for absolute calibration of SAR images as well. The type of targets that have so far been used for calibration using distributed targets are agricultural fields, tropical rain forests and boreal forests.

3. CALIBRATION OF NASA/JPL DC-8 SAR DATA

In Figure 2, is shown one of the first L-Band images of the Rosamond calibration site, near Edwards Air Force Base, collected in June 1990. This site is routinely used for external calibration of the NASA/JPL DC-8 SAR. The lake bed covers most of the DC-8 SAR swath, being ~8km wide. A fixed array of 2.45m trihedral corner reflectors of nearly uniform construction is deployed at one side of the lake bed. This array is clearly seen in the figure as a line of bright dots.

In Figure 3, we show typical radiometric variations across the swath extracted from the Rosamond data. These results were obtained from analysis of the trihedral corner reflector signatures after a radiometric bias had been removed from the entire data set. The results presented are estimated peak radar cross-section for the reflectors - the array is configured with each reflector pointing at a 45 degree boresite angle, so we have to use a model of the trihedral cross-section variation with elevation angle to estimate the peak RCS for each. Typical signal-to-background ratios for the trihedrals are better than 40dB at L- and C-Band and 30dB at P-band, which means that the clutter background is *not* a significant source of error for these measurements. The remaining sources of error are in the model of the trihedral RCS variation and any uncertainties in the radiometric correction applied in the standard SAR processing. From the figure, it can be seen that the HH-VV channel amplitude balance is excellent for L-and C-band, but varies significantly across the swath for P-band. Whether the source of the variation at P-band is caused by the reflectors or the system is not known. In Table 1, the root-mean-square (RMS)

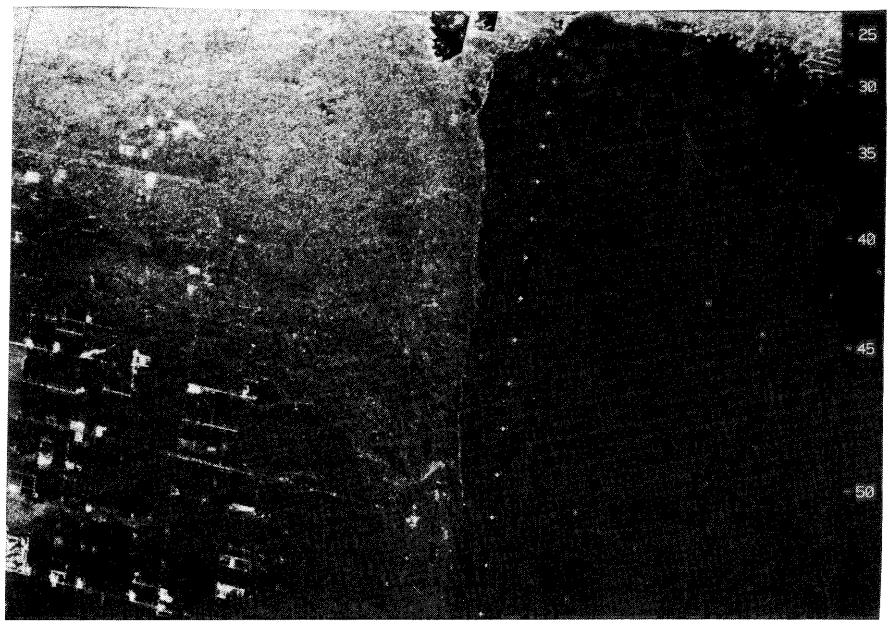

Figure 2. NASA/JPL DC-8 L-Band SAR image of the Rosamond dry lake bed calibration site.

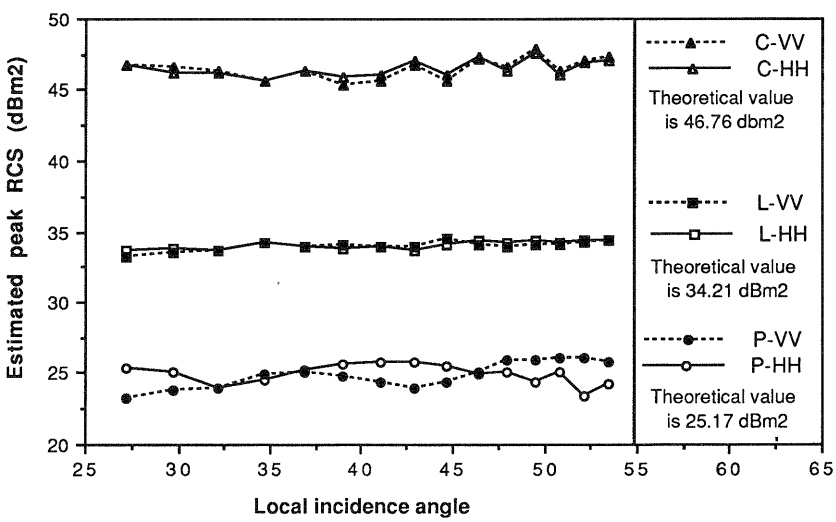

Figure 3. Radar cross-section measurements of trihedral corner reflectors at HH and VV polarizations from NASA/JPL DC-8 SAR image data of Rosamond dry lake bed calibration site.

and peak-to-peak variations in the estimated peak trihedral RCS values are given. The radiometric variations across the swath are consistent with the goal of ±1dB for SIR-C.

Long-term Stability

The calibration performance of the DC-8 SAR system has been monitored closely during the 1989 and 1990 flight seasons. In Table 2, some results of that analysis are presented. The results are average bias or offsets for the scattering matrix data determined from corner reflector signatures within each of the scenes analyzed. The bias or offsets, given in dB, should be subtracted from any of the backscatter (power) measurements obtained from the data. The results presented in the table show that, radiometrically, the DC-8 SAR system was stable to within ±1.2dB at L-Band, ±1dB at C-Band and P-Band HH, and ±1.9dB at P-Band VV over that time. These numbers do *not* include short-term variations across the swath, as given in Figure 3.

	RMS	Peak-to-peak
L-BAND HH	±0.3dB	±0.4dB
VV	±0.3dB	±0.7dB
C-BAND HH	±0.6dB	±0.9dB
VV	±0.8dB	±1.3dB
P-BAND HH	±0.7dB	±1.2dB
VV	±1.0dB	±1.4dB

Table 1: Radiometric variations across the swath from Rosamond trihedral data

		L-band		C-band		P-band	
Site name	Date	HH	VV	HH	VV	HH	VV
Flevoland	8/89	15.7	15.3	17.4	17.5	16.2	14.2
DLR	8/89	16.6	16.7	18.6	18.3	-	-
Mt. Shasta 1	9/89	18.1	-	17.9	-	15.6	-
Mt. Shasta 2	9/89	17.6	-	18.4	-	17.0	-
Goldstone 1	9/89	17.0	17.0	17.3	17.1	16.0	16.0
Goldstone 2	3/90	17.5	17.3	17.3	17.3	17.6	17.5
Rosamond	6/90	16.8	16.9	18.7	19.1	17.4	18.0
Mid-range (±Variation) (±1.9)		16.9 (±1.2)	16.3 (±1.0)	18.0 (±0.7)	18.1 (±1.0)	16.5 (±0.9)	16.1

Table 2: Bias or offsets for scattering matrix data in dB from long-term analysis of corner reflector signatures

The results presented in Table 3 suggest that the DC-8 system is sufficiently stable over the long term that a single set of radiometric calibration factors could be applied to convert the standard data products to σ^o.

4. RADIOMETRIC CORRECTION OF SAR IMAGES OF VARYING TERRAIN HEIGHT

Radiometric correction of SAR images of varying terrain heights to convert image pixel values to normalized radar cross-section (σ^o) via the SAR radar equation is an important goal in calibrating SAR images. Two major problems can occur in applying a radiometric correction to a given pixel value: the first is that if the elevation angle between the radar and the pixel location is wrong, then the correction for the SAR cross-track antenna pattern will be in error; the second is that if the local incidence angle for that pixel is wrong, the correction for the projection of the pixel area from slant range to ground range coordinates will be in error.

It can be seen from the above that radiometric variations of less than 0.3dB within an image are achievable in the case of airborne SAR data. However, much of the work done on calibrating airborne SAR data has been carried out in areas such as Rosamond which are relatively flat. There is an inherent problem in applying the calibration parameters obtained over flat areas to airborne SAR data obtained over areas with significant terrain height variations. The problem arises from the fact that it is not possible to determine the elevation angle for a given pixel when significant terrain height variations occur in the scene, unless the terrain height variations are known.

By examining the radar equation for the power, P_I, present in an uncalibrated SAR image pixel of size p_a meters in azimuth and p_r meters in slant range, due to a target of normalized radar cross-section σ^o, the problem can easily be seen. An appropriate (simplified) form of the radar equation is:

$$P_I = \frac{P_t G_t(\theta_{el}) G_r(\theta_{el}) \lambda^2 \sigma^o p_a p_r G_p(R) G_R}{(4\pi)^3 R^4 \sin\theta_i} \qquad (8)$$

where P_t = radar peak transmitted power, $G_t(\theta_{el})$ and $G_r(\theta_{el})$ are the gains of the receive and transmit antennas towards the target elevation angle, θ_{el}, G_p is the processor gain (range-dependent), λ the radar wavelength, G_r the receiver electronic gain (including any system losses), R the slant range to the target and $\sin\theta_i$ the sine of the local incidence angle (to take care of the projection of the pixel area on to the physical ground area). The SAR image can be radiometrically calibrated by dividing the power in each pixel by a factor $K(R,\theta_{el},\theta_i)$ to give σ^o, i.e.,

$$\sigma^o = \frac{P_I}{K(R,\theta_{el},\theta_i)}$$

$$\text{with } K = \frac{P_t G_t(\theta_{el}) G_r(\theta_{el}) \lambda^2 \sigma^o p_a p_r G_p(R) G_R}{(4\pi)^3 R^4 \sin\theta_i} \qquad (9)$$

or an estimate thereof. A common assumption for airborne SAR's is that the radar is viewing a flat earth. In this case,

$$\theta_{el} = \theta_i$$
$$\text{and } \theta_i = \cos^{-1}(h/R) \qquad (10)$$

where h is the height of the platform above the terrain. h is often determined by a radar altimeter or barometric altitude instrument. The flat earth assumption can easily break down if the radar is imaging a flat region but flying over a mountainous area, in which case the true height of the platform and the height as measured by an altimeter can differ significantly. This leads to poor estimates of the

elevation angle θ_{el} and the incidence angle θ_i and thus to poor estimates of the radiometric correction factor, K. This can cause very large radiometric errors in the SAR image, varying across the image.

In general , where the imaged terrain varies in height significantly as a function of image position (range and azimuth) the height of the platform above each pixel must be determined to find the appropriate elevation angle, θ_{el}, for correcting the antenna gains. Also, the slope of each pixel must be determined, to find θ_i and correct for the sine of local incidence angle term. The latter is a well known problem in radargrammetry (Leberl, 1990). We note that, in this more general case, θ_i and θ_{el} need not be the same. We also note that, for a spaceborne SAR, where the platform altitude is greater than, say, 250 km, the effect of terrain height variations on the determination of the elevation angle is less severe.

In the airborne SAR case, there are several possible solutions to the above problem. One is to use a Digital Elevation Model (DEM) for each imaged site and register it to the SAR image, then determine θ_{el} and θ_i for each pixel. Another approach would be to use stereo or interferometric SAR to generate a pixel by pixel elevation map and then determine θ_{el} and θ_i from that. A monopulse approach (Freeman and Zink, 1991) can be used to determine elevation angles (but not incidence angles) in SAR images.

Using Digital Elevation Models

The problem of matching DEM'S to radar images is well-known (Leberl, 1990). A commonly adopted strategy is to simulate the radar image from the DEM, using knowledge of the radar flight track, illumination geometry, and assuming some backscatter vs. incidence angle law for the imaged terrain. Then features in the simulated image and the actual radar image are compared and a web of "correspondence points" is established. This web is used to warp the simulated image to fit the radar image. The same warping process is applied to the DEM to register it to the radar image. Once the DEM and the radar image have been registered, elevation and incidence angles can be calculated for each image pixel and the image data can be properly radiometrically corrected.

Unfortunately, DEM's of sufficiently high resolution are not available for all of the earth's surface and, for those areas that are covered, the process of registering the DEM to the SAR image can be difficult if adequate tie-points can not be found, and is currently costly and labor intensive. Difficulties may also occur when the terrain cover changes, e.g. from grass or bare soil to trees, so that the backscatter vs. incidence angle behavior is not constant over the image.

Using Interferometry

Interferometry using airborne SAR is best done with two coherent SAR antennas mounted on the same platform, displaced in the across-track dimension by a known distance. It can also be achieved using very precise repeat tracks of the aircraft, but the requirements on the closeness of the repeat tracks are very strict and the radar backscatter returns may decorrelate quickly due to wind motion or rain, for example. Stereo SAR requires two passes over the same site at different look angles and for the track of the airborne platform to be well known in order to precisely register the two resulting images.

At JPL, a dual-antenna across-track SAR interferometer operating at C-band called TOPSAR has been developed jointly with the Italian Space Agency (Zebker et al, 1992), and integrated into the NASA/JPL DC-8 airborne SAR system. The TOPSAR interferometer produces interferometric SAR images and very precise height maps which are have the same imaging geometry as the standard L- and P-band polarimetric SAR images produced by the DC-8 SAR. This means that registration of the height map and the SAR images and generation of the elevation and incidence angle maps which correspond to the SAR image pixels is straightforward, and involves no warping process. The only disadvantage to this approach is that currently, the TOPSAR images cover only a half of the swath width of the standard DC-8 SAR data products. This means that proper radiometric correction for terrain height variations can only be applied to half of the standard DC-8 SAR images.

Using the Monopulse Approach

(Freeman and Zink, 1991) have presented an approach for determining elevation angles from SAR data using the monopulse principle. The approach begins with the observation that, provided like- and cross-polarized backscatter are uncorrelated, then the algorithm described in (van Zyl, 1989) for calculating antenna cross-talk yields a measurable quantity whose amplitude (and phase) depends only on elevation angle (or off-boresight angle). Thus, if the cross-talk for a given point in the image is determined, that measurement can be related to the elevation angle appropriate to that point. Knowledge of the slant range to the point then allows determination of the height of the platform above it. This operation, repeated at many locations throughout the image, allows one to

build up a low-resolution topographic map of the height of the aircraft above each location. If a dedicated monopulse antenna is available, there is no need to use the cross-talk approach described above, and better resolution results can be obtained.

The major disadvantage of the monopulse approach is that the technique as currently implemented does not give sufficiently fine resolution in the topographic map to allow the local incidence angle for each pixel to be properly determined. Thus the sin θ_l term in (9) can not be corrected for using this approach. The sin θ_l term is , however, scene-dependent: the monopulse approach does allow the removal of all system-dependent radiometric variations in the image so that the data can be converted to radar cross section, σ (but not σ^o), and may be useful where height maps from interferometric SAR or DEM's are not available.

5. ERS-1 SAR DATA CALIBRATION

ERS-1 has been transmitting SAR data to the Alaska SAR Facility (ASF) since early August, 1991, averaging over 36 minutes of data per day. Calibration transponders and trihedral corner reflectors have been deployed in two locations along one of the descending flight tracks in Alaska during the commissioning phase, which ended December 15, 1991. Over 25 over flights have imaged these calibration sites. Standard SAR calibration measurements have been made of full resolution, low resolution, and complex image products. These include measurements of resolution, PSLR, noise equivalent normalized radar cross section, number of looks, and image geolocation accuracy. Semi-automated software has been developed to facilitate these analyses. The radiometric stability of the SAR data produced by ASF has been analyzed over a several hundred kilometer baseline as well as over a period of four months. Absolute radiometric correction factors have been estimated to within 2 dB.

Radiometric Calibration

Within a single image, the cross-track radiometric compensation applied during the post-processing phase to both full resolution and complex images reduces intrinsic relative calibration inaccuracies to less than 0.2 dB. This radiometric compensation vector, principally consists of range attenuation compensation modulated by the inverse of the ERS-1 cross-track antenna pattern, shown in Figure 4. This antenna pattern varies by 1.3 dB across the swath. Figure 4 contains the points used to fit an estimated fourth-order curve to the data, together with the antenna pattern as measured before launch, which was supplied by ESA after the bulk of the calibration effort during the commissioning phase for ERS-1 had been completed. The fitted and measured curves differ by less than 0.32 dB. Along-track radiometric accuracy is affected by potential system instabilities in the radar. Based on point target and noise measurements, an along-track upper bound of 0.2 dB also applies to the along-track radiometric stability of the ECISAR.

Pass to pass radiometric stability for the ERS-1 data is also excellent. Analysis of imaging transects of the state of Alaska separated by three days in early September show that boreal forests in the Alaskan interior are good candidates for assumed radiometric stability, at least during the seasons covered by the commissioning phase. This is in contrast to tundra on the North Slope, which can exhibit strong backscatter changes in response to temperature fluctuations as described below. The boreal forests exhibit radiometric stability to within .3 dB from September 11 through 14. The variations in return power are attributable either to radar system instability or to physical processes which alter the backscatter properties of the terrain. Thus from this measurement, .3 dB is an upper limit on the pass-to-pass relative calibration of the image data. The possibility of mutually compensatory error sources was eliminated through the analysis of stable river drainages on the North Slope during the same time period.

Absolute calibration is determined by comparison of a trihedral corner reflector's integrated image power with its theoretical radar cross section. This task has met with some difficulty due to the difficult nature of deployment of the trihedrals in the Alaskan Interior and on the North Slope. The rigors of transport to calibration sites and the harsh conditions at those sites have contributed an estimated 2 dB degradation in effective trihedral radar cross section. Consequently the uncertainty in absolute calibration is 2 dB. This correction has been assimilated into the ASF Data User's Guide.

Noise Equivalent sigma-zero

The noise-equivalent sigma-zero in the images has been estimated by looking at the 'backscatter' values for very dark targets, such as the numerous lakes in our two calibration site areas (see Figure 5, for example). The noise-equivalent sigma-zero is estimated to be -24.7 ($\pm$1.5)dB at the center of the imaged swath.

SUMMARY

Radiometric calibration of SAR image data using a variety of different approaches is now becoming part of the operational data generation. Two SAR sensors, the NASA/JPL DC-8 SAR and ESA's ERS-1 are producing routinely calibrated SAR image data. The next step is for the remote sensing community to take advantage of the opportunities offered by these data and use calibrated SAR images in their natural role, which is in monitoring temporal change on the earth's surface.

ACKNOWLEDGMENTS

The research described in this paper was carried out by the Jet Propulsion Laboratory, California Institute of Technology under a contract with the National Aeronautics and Space Administration. The author would like to thank the aircraft group, Rob Fatland and Tom Bicknell of JPL and Shusun Li and Tom George of ASF for their invaluable assistance in providing data and results.

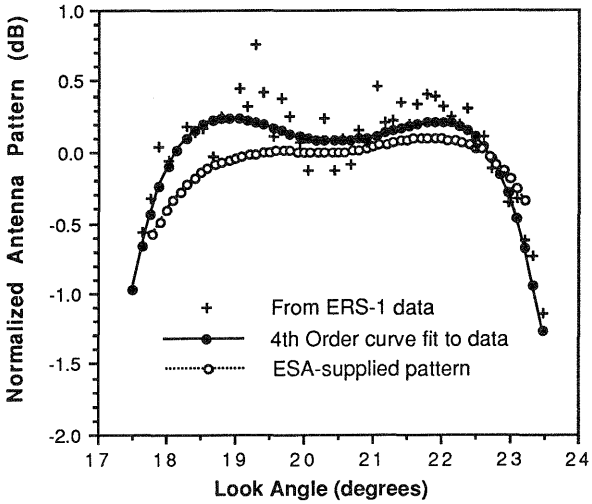

Figure 4. ERS-1 Antenna Pattern derived from calibration site data and as supplied by ESA

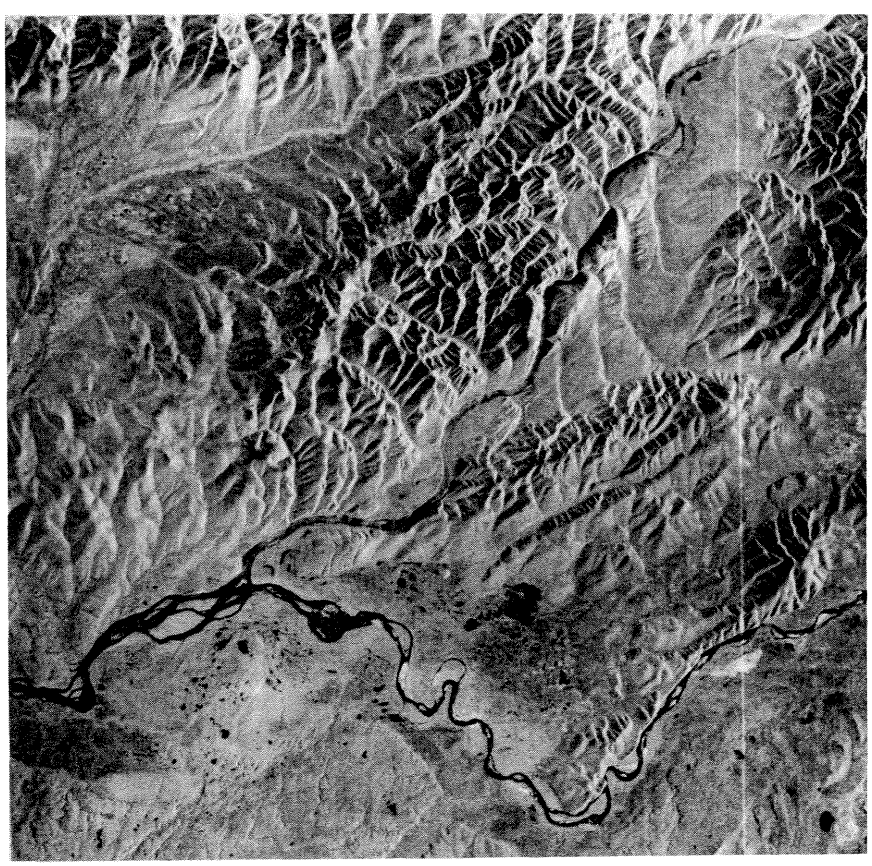

Figure 5: ASF ERS-1 SAR image of Tanana River, Alaska calibration site

REFERENCES

Attema, E.P.W., 1991. "The Active Microwave Instrument On-Board the ERS-1 Satellite", Proc. IEEE, Vol. 79, No.6, pp. 791-799, June 1991.

Currie, N.C. (ed.), 1984. Techniques of Radar Reflectivity Measurement, Artech House, 1984.

Elachi, C., Im, E., Roth, L.E. and Werner, C.L., 1991. "Cassini Titan Radar Mapper", Proc. IEEE, Vol. 79, No.6, pp. 867-880, June 1991.

Ford, J. P., et al, 1980. "Seasat views North America, The Caribbean and Western Europe with Imaging Radar", JPL Publication No. 80-67, November 1980.

Freeman, A., Curlander, T. C. Dubois, P.D. and Klein, J. D., 1988. "SIR-C Calibration Workshop Report", JPL Center for Radar Studies publication No. 88-003, JPL Publication # D-6165, November 1988.

Freeman, A. and Curlander, J.C., 1989. "Radiometric Correction and Calibration of SAR Images", Photogrammetric Engineering & Remote Sensing, Vol. 55, No. 9, September 1989, pp. 1295-1301.

Freeman, A., Shen, Y. and Werner, C.L., 1990. "Polarimetric SAR Calibration Experiment Using Active Radar Calibrators", IEEE Trans. on Geoscience and Remote Sensing, Vol. GE-28, No. 2, March 1990.

Freeman, A., van Zyl, J.J., Klein, J.D., Zebker, H.A. and Shen, Y., 1991. "Calibration of Stokes and scattering matrix format polarimetric SAR data", accepted for publication in IEEE Trans. on Geoscience and Remote Sensing, 1991.

Freeman, A. and Zink, M., 1991. Application of the Monopulse Principle to determining Elevation Angles in SAR images, submitted to IEEE Trans. on Geoscience and Remote Sensing, December 1991.

Gray, A.L., Vachon, P.W., Livingstone, C.E. and Lukowski, T.I., 1990. "Synthetic Aperture Radar Calibration Using Reference Reflectors", IEEE Trans. on Geoscience and Remote Sensing, Vol.GE-31, No. 3, May 1990, pp 374-383.

Held, D.N., et al, 1988. "The NASA/JPL multifrequency, multipolarization airborne SAR system", Proc. IGARSS '88, Edinburgh, Scotland, pp. 345-349, 1988.

Johnson, W.T.K., 1991. "Magellan Imaging Radar Mission to Venus", Proc. IEEE, Vol. 79, No.6, pp. 777-790, June 1991.

Jordan, R.L., Huneycutt, B.L. and Werner, M., 1991. "The SIR-C/X-SAR Synthetic Aperture Radar System", Proc. IEEE, Vol. 79, No.6, pp. 827-838, June 1991.

Leberl, F.W., 1990. Radargrammetric Image Processing, publ. Artech House, 1990.

Nemoto, Y., Nishino, H., Ono, M., Mizutamari, H., Nishikawa, K. and Tanaka, K., 1991. "Japan Earth Resources Satellite-1 Synthetic Aperture Radar", Proc. IEEE, Vol. 79, No.6, pp. 800-809, June 1991.

Moore, R.K. and Hemmat, M., 1988. "Determination of The Vertical Pattern of the SIR-B Antenna", Int. J. Remote Sensing, Vol. 9, No. 5, May 1988, pp. 839-848.

Raney, R.K., 1980. "SAR response to partially coherent phenomena", IEEE Trans. on Antennas and Propagation, Vol. AP-28, No.6, pp. 777-787, November 1980.

Raney, R.K., Luscombe, A.P., Langham, E.J. and Ahmed, S., 1991. "RADARSAT", Proc. IEEE, Vol. 79, No.6, pp. 839-849, June 1991.

Ulaby, F.T., Moore, R.K. and Fung, A.K., 1989. "Microwave Remote Sensing: Active and Passive", Vol.'s I, II and III, Addison-Wesley, 1981-1989.

Ulaby, F.T. and Elachi, C. (ed.), 1990. "Radar Polarimetry for Geoscience Applications", Artech House, 1990.

van Zyl, J.J., 1990. "Calibration of Polarimetric Radar Images Using Only Image Parameters and Trihedral Corner Reflector Responses", IEEE Trans. on Geoscience and Remote Sensing, Vol. GE-28, No.3, pp. 337-348, May 1990.

Wiley, Carl A.,1954. "Pulsed Doppler Radar Methods and Apparatus", U.S. Patent 3,196,436, Filed August 13, 1954, patented July 20, 1965.

Zebker, H. A., Madsen, S. N. and Martin, J., 1992. The TOPSAR Interferometric Radar Topographic Mapping System, Proc. IGARSS '92.